Fast-ion energy resolution by one-step reaction gamma-ray spectrometry

Salewski, Mirko; Nocente, M.; Gorini, G.; Jacobsen, Asger Schou; Kiptily, V.G.; Korsholm, Søren Bang; Leipold, Frank; Madsen, Jens; Moseev, Dmitry; Nielsen, Stefan Kragh

Total number of authors:
13

Published in:
Nuclear Fusion

Link to article, DOI:
10.1088/0029-5515/56/4/046009

Publication date:
2016

Document Version
Peer reviewed version

12 December 2016

Fast-ion energy resolution by one-step reaction gamma-ray spectrometry

M. Salewski[1], M. Nocente[2,3], G. Gorini[2,3], A.S. Jacobsen[1], V.G. Kiptily[4], S.B. Korsholm[1], F. Leipold[1], J. Madsen[1], D. Moseev[5], S.K. Nielsen[1], J. Rasmussen[1], M. Stejner[1], M Tardocchi[3] and JET Contributors[6]‡

[1] Technical University of Denmark, Department of Physics, DK-2800 Kgs. Lyngby, Denmark

[2] University of Milano Bicocca, Department of Physics, Milano 20126, Italy

[3] Istituto di Fisica del Plasma, Consiglio Nazionale delle Ricerche, Milano 20125, Italy

[4] CCFE, Culham Science Centre, Abingdon, Oxon, X14 3DB, UK

[5] Max Planck Institute for Plasma Physics, 17491 Greifswald, Germany

[6] EUROfusion Consortium, JET, Culham Science Centre, Abingdon, OX14 3DB, UK

E-mail: `msal@fysik.dtu.dk`

Abstract. The spectral broadening of γ-rays from fusion plasmas can be measured in high-resolution gamma-ray spectrometry (GRS). We derive weight functions that determine the observable velocity space and quantify the velocity-space sensitivity of one-step reaction high-resolution GRS measurements in magnetized fusion plasmas. The weight functions suggest that GRS resolves the energies of fast ions directly without the need for tomographic inversion for selected one-step reactions at moderate plasma temperatures. The D(p,γ)^{3}He reaction allows the best direct fast-ion energy resolution. We illustrate our general formalism using reactions with and without intrinsic broadening of the γ-rays for the GRS diagnostic at JET.

1. Introduction

Resolution of the energies of fast particles in fusion plasmas is a long-standing problem in present energetic-particle diagnostics. For example, the ITER measurement requirements entail resolution of the energy spectrum of confined α-particles [2]. However, recent studies of the velocity-space sensitivity of available core plasma fast-ion diagnostics suggest that this goal cannot be achieved by traditional measurements and analysis techniques as there is no direct one-to-one correspondence between fast-ion energy and measured signals [3–8]. In fact, fast-ion charge-exchange recombination spectroscopy (e.g. fast-ion D_α (FIDA) [3,4]), collective Thomson scattering (CTS) [4,5], neutron emission spectrometry (NES) [6, 7] and two-step reaction γ-ray spectrometry

‡ See the Appendix of [1]

(GRS) [8] are not sensitive to distinct energies or pitches but to large regions in 2D velocity space covering a wide range of energies and pitches. Neutral particle analyzers (NPA) are a notable exception and resolve fast-ion energies for the observable narrow pitch range [3]. Here we demonstrate that fast-ion energies for all pitches can be resolved directly by one-step reaction GRS. However, good direct energy resolution is achievable only for selected one-step reactions, such as the D(p,γ)^{3}He reaction with fast protons. Further, the plasma temperature needs to be moderate. Hence direct energy resolution in burning plasmas in ITER remains elusive. Nevertheless, energy resolution of fast ions is possibly achievable by tomographic inversion in velocity space [9–13].

In GRS the γ-rays emitted by fusion plasmas are spectrally analyzed [14, 15]. Today the highest γ-ray fluxes from fusion plasmas are achieved at JET where GRS is routinely used [16–32]. The high nuclear reaction rates in the upcoming DT campaign at JET [1, 33] and later in burning plasmas at ITER and DEMO will further enhance the γ-ray emission [14, 15, 34, 35]. GRS measurements have traditionally been made at moderate spectral resolution just sufficient to identify peaks appearing at characteristic γ-ray energies in the spectra. Each peak can be related to a nuclear reaction by the γ-ray energy. GRS measurements at moderate spectral resolution have been made at Doublet-III [36], TFTR [37], JET [16–24] and JT-60U [38, 39]. New detectors [27, 40] allow GRS measurements at very high spectral resolution sufficient to resolve the spectral shapes of the individual peaks as demonstrated at JET [25–31] and ASDEX Upgrade [41].

Nuclear reactions emitting γ-rays can be divided into one-step reactions and two-step reactions based on their reaction kinematics [14]. In one-step reactions the γ-ray is a primary reaction product, as e.g. in D(p,γ)^{3}He which can also be written as

$$\mathrm{D} + \mathrm{p} \rightarrow {}^3\mathrm{He} + \gamma. \tag{1}$$

In two-step reactions the γ-ray is a secondary reaction product, as e.g. in ^{9}Be(α, nγ)^{12}C. The two steps of this reaction are:

$$\alpha + {}^9\mathrm{Be} \rightarrow {}^{12}\mathrm{C}^* + \mathrm{n}, \tag{2}$$

$$^{12}\mathrm{C}^* \rightarrow {}^{12}\mathrm{C} + \gamma. \tag{3}$$

As this reaction releases high γ-ray fluxes in tokamaks with strong alpha particle populations and beryllium as a main plasma impurity, it is foreseen for alpha particle studies in the upcoming DT campaign at JET and at ITER [19, 42].

We have recently shown that two-step reaction high-resolution GRS measurements observe rather large regions in velocity space [8]. The measurements are sensitive to energies near the nuclear resonances in selected pitch ranges. As γ-rays at measured energies E_γ can be produced on several nuclear resonances, two-step reaction GRS actually provides no direct resolution of fast-ion energies. Here we demonstrate that selected one-step reaction GRS measurements, on the contrary, directly provide resolution of the fast-ion energies at moderate plasma temperatures. We will consider the D(p,γ)^{3}He reaction as the main example as well as the reactions summarized in table 1.

Table 1. One-step fusion reactions discussed in this paper. The Q-value is the energy released in the reaction. σ_Q stands for the intrinsic non-zero mass width of the nuclear reaction product.

Reaction	Q [MeV]	σ_Q [MeV]	Remark
D(p,γ)^{3}He	5.5	0.0	well-established cross sections, often analysed
D(D,γ)^{4}He	23.8	0.0	peak has not been found at JET
D(T,γ)^{5}He	16.85	0.648	intrinsic broadening
T(p,γ)^{4}He	19.7	0.0	suggested for DEMO, good for H in DT plasma

The sensitivity in 2D velocity-space of fast-ion diagnostics can be described by weight functions. At present, weight functions have been developed for FIDA [3, 4], NPA [3], CTS [4, 5], fast-ion loss detectors [43] and NES [6, 7] as well as for two-step reaction GRS [8]. Weight functions have been used in four ways. First, they show the velocity-space sensitivity of the diagnostic separating the observable velocity-space regions from unobservable regions [3–8, 31, 44–63]. Second, assuming a 2D fast-ion velocity distribution function, the velocity-space distribution of the ions generating a given measurement can be calculated [3–8, 31, 44, 57–62, 64]. Third, they allow rapid calculation of synthetic measurements [4–8]. Fourth, given enough measurements and sufficiently high signal-to-noise ratio, it is possible to infer 2D fast-ion velocity distribution functions by tomographic inversion [5, 9–13, 65, 66]. The formalism we present here allows these applications for one-step reaction GRS measurements.

This paper is organized as follows. In section 2 we consider the kinematics of one-step reactions. In section 3 we present analytic weight functions describing the velocity-space sensitivity of high-resolution one-step reaction GRS measurements. Section 4 illustrates typical observable velocity-space of the GRS spectrometer at JET for the D(p,γ)^{3}He reaction. In section 5 we derive analytic expressions for the boundaries of the observable regions and explain the energy resolution of one-step reaction GRS by energy and momentum conservation. In section 6 we benchmark our formalism against numerical simulations. Section 7 discusses other nuclear reactions with and without so-called intrinsic broadening. Similarly, in section 8 the impact of thermal broadening is discussed. Finally, in section 9 we discuss implications of our formalism, and in section 10 we draw conclusions.

2. Kinematics of one-step reactions

The reaction kinematics determines the spectral broadening of the peak in the spectrum for reactions without intrinsic broadening [67]. Here we derive the relationship between the line-of-sight velocity u_f, the energy of the fast ion and the energy E_γ of the detected γ-ray by considering the reaction kinematics. As u_f depends on the gyroangle Γ of the fast ion, we can relate the energy E_γ to the gyroangle Γ of the fast ion. For a generic one-step reaction between species 1 and species 2 to form a reaction product,

pr, releasing a γ-ray, the non-relativistic energy and momentum conservation equations are, respectively,

$$\frac{1}{2}m_1v_1^2 + \frac{1}{2}m_2v_2^2 + Q = \frac{1}{2}m_{pr}v_{pr}^2 + E_\gamma, \tag{4}$$

$$m_1\mathbf{v}_1 + m_2\mathbf{v}_2 \qquad = m_{pr}\mathbf{v}_{pr} + \mathbf{p}_\gamma. \tag{5}$$

E_γ and $\mathbf{p}_\gamma$ are respectively the energy and momentum of the emitted γ-ray, and Q is the energy released in the reaction. We now assume that one species is fast and the other thermal. Neglecting the energy and momentum of the thermal species and denoting the mass of the fast species to m_f and its velocity to $\mathbf{v}_f$, the energy and momentum equations become

$$\frac{1}{2}m_fv_f^2 + Q = \frac{1}{2}m_{pr}v_{pr}^2 + E_\gamma, \tag{6}$$

$$m_f\mathbf{v}_f \qquad = m_{pr}\mathbf{v}_{pr} + \mathbf{p}_\gamma. \tag{7}$$

The effects of non-zero temperature will be calculated in section 8 using the GENESIS code [29,68]. Elimination of v_{pr}^2 in equation 6 using equation 7 gives

$$\frac{1}{2}m_fv_f^2 + Q = \frac{1}{2m_{pr}}\Big(m_f^2v_f^2 - 2m_f\mathbf{p}_\gamma\cdot\mathbf{v}_f + p_\gamma^2\Big) + E_\gamma \tag{8}$$

where $p_\gamma = |\mathbf{p}_\gamma|$. Equation 8 could also be obtained from the erroneous equation $m_f\mathbf{v}_f = -m_{pr}\mathbf{v}_{pr} + \mathbf{p}_\gamma$ instead of momentum conservation (equation 5). This is checked for and excluded below. The dot product $\mathbf{p}_\gamma\cdot\mathbf{v}_f$ can be expressed in terms of the line-of-sight velocity u_f by introducing the unit vector along the line-of-sight $\hat{\mathbf{p}}_\gamma$:

$$\mathbf{p}_\gamma\cdot\mathbf{v}_f = p_\gamma\hat{\mathbf{p}}_\gamma\cdot\mathbf{v}_f = p_\gamma u_f. \tag{9}$$

The magnitude of the momentum p_γ and the energy of the γ-ray are related by

$$p_\gamma = E_\gamma/c \tag{10}$$

where c is the speed of light. Substitution of equations 9 and 10 into equation 8 gives

$$\frac{1}{2}m_fv_f^2 + Q = \frac{1}{2m_{pr}}\Big(m_f^2v_f^2 - 2m_f\frac{E_\gamma}{c}u_f + \frac{E_\gamma^2}{c^2}\Big) + E_\gamma. \tag{11}$$

Equation 11 relates the line-of-sight velocity u_f of the fast ion to the measurable energy E_γ of the γ-photon. We solve equation 11 for u_f and express v_f^2 in $(v_\parallel, v_\perp)$-coordinates with respect to the total magnetic field as $v_f^2 = v_\parallel^2 + v_\perp^2$:

$$u_f = \frac{(m_f - m_{pr})c}{2E_\gamma}(v_\parallel^2 + v_\perp^2) + \frac{E_\gamma}{2m_fc} + \frac{m_{pr}c(E_\gamma - Q)}{m_fE_\gamma}. \tag{12}$$

The line-of-sight velocity u_f is determined by the gyroangle Γ according to [5,7,11]

$$u_f = v_\parallel\cos\phi + v_\perp\sin\phi\cos\Gamma \tag{13}$$

where ϕ is the observation angle between the line-of-sight and the magnetic field. We eliminate u_f from equations 12 and 13 and solve for $\Gamma\in[0,\pi]$:

$$\Gamma = \arccos\frac{\frac{(m_f-m_{pr})c}{2E_\gamma}(v_\parallel^2 + v_\perp^2) + \frac{E_\gamma}{2m_fc} + \frac{m_{pr}c(E_\gamma-Q)}{m_fE_\gamma} - v_\parallel\cos\phi}{v_\perp\sin\phi}. \tag{14}$$

This relation allows us to calculate the gyroangle $\Gamma \in [0, \pi]$ of the fast ion leading to the detected energy E_γ of the γ-ray. A second solution for $\Gamma' \in [\pi, 2\pi]$ is given by [5]

$$\Gamma' = 2\pi - \Gamma. \tag{15}$$

3. One-step reaction GRS weight functions

The relation between fast-ion measurements, s, and fast-ion distribution functions, f, can be expressed as an integral over phase space,

$$s(E_{\gamma,1}, E_{\gamma,2}, \phi) = \int_{vol} \int_0^\infty \int_{-\infty}^\infty w(E_{\gamma,1}, E_{\gamma,2}, \phi, v_\parallel, v_\perp, \mathbf{x}) f(v_\parallel, v_\perp, \mathbf{x}) dv_\parallel dv_\perp d\mathbf{x} \tag{16}$$

where w is the weight function [3–8, 44] and $\mathbf{x}$ denotes the spatial coordinates. For GRS measurements, $s(E_{\gamma,1}, E_{\gamma,2}, \phi)$ is the detection rate of γ-rays [photons/s] in the energy range $E_{\gamma,1} < E_\gamma < E_{\gamma,2}$ with an observation angle ϕ. The units of $f(v_\parallel, v_\perp, \mathbf{x})$ are [fast ions $\times$ s^2/m^5]. The units of GRS weight functions are thus [photons / (fast ion $\times$ s)] describing the velocity-space sensitivity of the diagnostic. Analogous to two-step reaction GRS weight functions as well as FIDA and NES weight functions [4, 7, 8], we factor GRS weight functions w into a detection rate function $R(v_\parallel, v_\perp, \phi, \mathbf{x})$ and a probability prob$(E_{\gamma,1} < E_\gamma < E_{\gamma,1} | \phi, v_\parallel, v_\perp)$:

$$w(E_{\gamma,1}, E_{\gamma,2}, \phi, v_\parallel, v_\perp, \mathbf{x}) = R(v_\parallel, v_\perp, \phi, \mathbf{x}) \times \text{prob}(E_{\gamma,1} < E_\gamma < E_{\gamma,2} | \phi, v_\parallel, v_\perp). \tag{17}$$

$R(v_\parallel, v_\perp, \phi, \mathbf{x})$ describes incident rates in [photons / (fast ion $\times$ s)] irrespective of the γ-ray energy [8]. $R(v_\parallel, v_\perp, \phi, \mathbf{x})$ hence has the same units as weight functions whereas the probabilities are dimensionless numbers between 0 and 1. The laws of energy and momentum conservation determine the boundaries of the probability functions prob$(E_{\gamma,1} < E_\gamma < E_{\gamma,2} | \phi, v_\parallel, v_\perp)$ in $(v_\parallel, v_\perp)$-space and hence ultimately the boundaries of weight functions which separate the observable regions from the unobservable regions.

Before we calculate probability functions, we briefly discuss the rate function R. Assuming a fast reactant with velocity $(v_\parallel, v_\perp)$ and a thermal reactant at rest and neglecting any angle dependence of the cross section σ, the rate function can be calculated according to [7]

$$R(v_\parallel, v_\perp, \mathbf{x}) = \frac{\Omega}{4\pi} n_t \sqrt{v_\parallel^2 + v_\perp^2} \sigma\Big(\sqrt{v_\parallel^2 + v_\perp^2}\Big). \tag{18}$$

where Ω is the solid angle of the detector as seen from position $\mathbf{x}$ and n_t is the density of the thermal ions. The cross section can be modelled as [41]

$$\sigma(E) = \frac{S}{E} \exp(-\beta_G / \sqrt{E}) \tag{19}$$

where $E = \frac{1}{2} m (v_\parallel^2 + v_\perp^2)$ is the energy (which depends on the velocity-space position), β_G is the Gamow constant and S is the so-called astrophysical factor which is a slowly varying function of energy [69, 70]. For the D(p,γ)^{3}He reaction, S is modelled as a fifth-order polynomial for which the coefficients are given in reference [41]. The rate function is illustrated in figure 1.

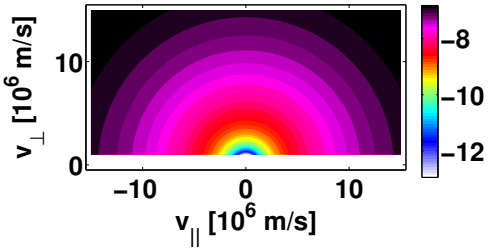

Figure 1. Rate function R in units [γ-photons / (ion $\times$ s)]. The magnitude is shown in base 10 logarithm.

The probability function $\mathrm{prob}(E_{\gamma,1} < E_\gamma < E_{\gamma,2}|\phi, v_\parallel, v_\perp)$ can be calculated by transforming to probabilities in Γ using equation 14. This transformation is advantageous as the gyroangle has, to a good approximation, a uniform distribution:

$$\mathrm{pdf}_\Gamma = \frac{1}{2\pi}. \tag{20}$$

We write the probability function as an integral over the corresponding probability density function and transform to probability densities in Γ:

$$\mathrm{prob}(E_{\gamma,1} < E_\gamma < E_{\gamma,2}|\phi, v_\parallel, v_\perp) = \int_{E_{\gamma,1}}^{E_{\gamma,2}} \mathrm{pdf}(E_\gamma|\phi, v_\parallel, v_\perp) dE_\gamma$$

$$= \int_{\Gamma_2}^{\Gamma_1} \mathrm{pdf}_\Gamma d\Gamma + \int_{2\pi-\Gamma_1}^{2\pi-\Gamma_2} \mathrm{pdf}_\Gamma d\Gamma = \frac{\Gamma_1 - \Gamma_2}{\pi}. \tag{21}$$

We have used that

$$\mathrm{pdf}(E_\gamma|\phi, v_\parallel, v_\perp) = \mathrm{pdf}_\Gamma \left| \frac{d\Gamma}{dE_\gamma} \right|. \tag{22}$$

The second integral in Γ arises due to the second solution in Γ shown in equation 15. The integration limits Γ_1 and Γ_2 are respectively given by the energies $E_{\gamma,1}$ and $E_{\gamma,2}$ according to equation 14. We stress that the probability function depends only on the observation angle ϕ, the considered γ-ray energy range and the reaction kinematics but not on the reaction cross sections.

4. Observable velocity-space regions for the D(p,γ)^{3}He reaction at JET

Typical observation angles for the two high-resolution GRS diagnostics at JET are about $\phi = 90°$ and $\phi = 30°$ with respect to the magnetic field in the plasma centre. The observation angle varies along the line-of-sight. However, as most γ-rays are generated in the plasma centre, we neglect these spatial variations here. Figure 2 shows probability functions for the D(p,γ)^{3}He reaction with fast protons and thermal deuterium for these angles and various γ-ray energy ranges. In this case the proton velocity is much larger than the deuterium velocity ($v_p \gg v_D$). This reaction is often studied for plasma scenarios with ICRH hydrogen minority heating in deuterium plasma [18, 41, 67]. The observation regions are similar for the two views and are bounded by circular arcs that

have their centers close to the origin as we will show in section 5. Hence fast ions in narrow energy ranges are observable in each γ-ray energy range. The radius of each circular arc as well as the distance of its center to the origin are independent of ϕ. For $\phi = 90°$ the probability functions are symmetric about $v_\parallel = 0$. For $\phi = 30°$ the center is tilted towards negative parallel velocities, and hence the observation regions are slightly biased towards negative parallel velocities. We also observe that the probability functions for $\phi = 30°$ are narrower and have larger amplitudes than those at $\phi = 90°$. The arcs for $\phi = 30°$ are narrower as the impact of the gyromotion is smaller according to equation 13. The shapes and amplitudes of the probability functions suggest good resolution of the fast ion energies for all pitches in contrast to other fast-ion diagnostics. Weight functions with perfect energy resolution would be bounded by concentric circular arcs about the origin in $(v_\parallel, v_\perp)$-coordinates.

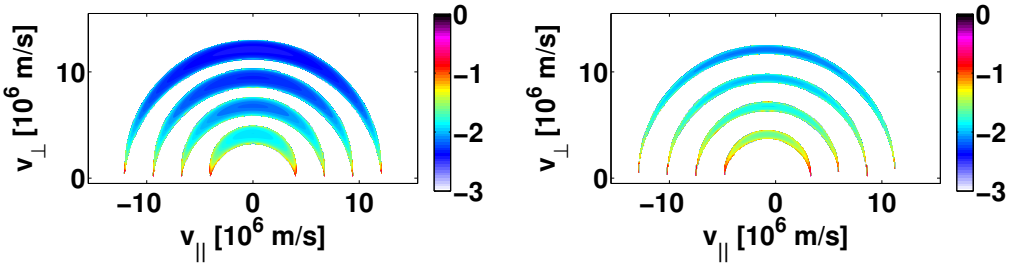

(a) $\phi = 90°$ (b) $\phi = 30°$

Figure 2. Probability functions prob$(E_{\gamma,1} < E_\gamma < E_{\gamma,2}|\phi, v_\parallel, v_\perp)$ of D(p,γ)^{3}He with $v_p \gg v_D$ for two observation angles ϕ and various γ-ray energies in base 10 logarithm. In each figure we plot four probability functions showing the observation regions at four γ-ray energy ranges with fixed width $E_{\gamma,2} - E_{\gamma,1} = 1$ keV. From inside to outside: $E_{\gamma,1} - Q = 50$ keV, 150 keV, 300 keV, 500 keV.

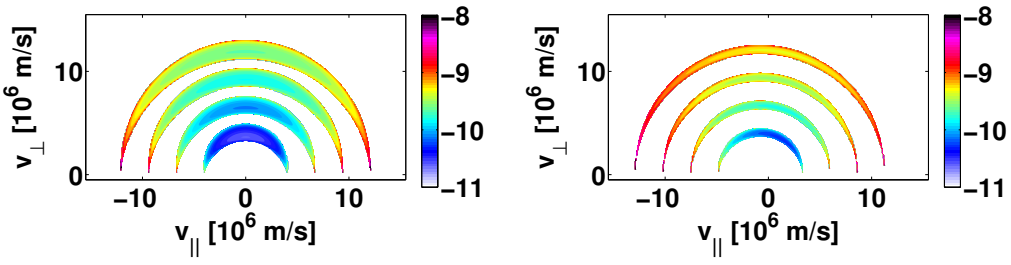

(a) $\phi = 90°$ (b) $\phi = 30°$

Figure 3. Weight functions of D(p,γ)^{3}He with $v_p \gg v_D$ for two observation angles ϕ and various γ-ray energy ranges of fixed width $E_{\gamma,2} - E_{\gamma,1} = 1$ keV in units [γ-photons / (ion $\times$ s)] in base ten logarithm. From inside to outside: $E_{\gamma,1} - Q = 50$ keV, 150 keV, 300 keV, 500 keV. The weight functions are obtained from equation 17. R is shown in figure 1 and prob$(E_{\gamma,1} < E_\gamma < E_{\gamma,2}|\phi, v_\parallel, v_\perp)$ in figure 2.

Figure 3 shows the corresponding weight functions, i.e. the product of each probability function from figure 2 with the rate function R from figure 1. As R covers

the entire velocity space, the forms of the probability functions and the corresponding weight functions are identical. However, as the cross sections and hence R increase with energy, the weight functions have their largest amplitudes in the parts furthest away from the origin.

5. Boundaries of one-step reaction GRS weight functions

Boundaries of weight functions are found by inserting $\cos\Gamma = \pm 1$ in equation 13 as then the line-of-sight velocity is at extremal values for given ϕ. Substitution of u_f into equation 12 then gives

$$\begin{aligned} &E_\gamma^2 + 2m_{pr}c^2(E_\gamma - Q) - 2m_f c(v_\parallel \cos\phi \pm v_\perp \sin\phi)E_\gamma \\ &-m_f(m_{pr} - m_f)c^2(v_\parallel^2 + v_\perp^2) = 0. \end{aligned} \tag{23}$$

Equation 23 can be written in the form $(v_\parallel - v_{\parallel,0})^2 + (v_\perp - v_{\perp,0})^2 = r_v^2$:

$$\begin{aligned} &\left(v_\parallel + \frac{\cos\phi E_\gamma}{(m_{pr} - m_f)c}\right)^2 + \left(v_\perp \pm \frac{\sin\phi E_\gamma}{(m_{pr} - m_f)c}\right)^2 \\ &= \frac{m_{pr}E_\gamma^2 + 2m_{pr}(m_{pr} - m_f)c^2(E_\gamma - Q)}{m_f(m_{pr} - m_f)^2c^2}. \end{aligned} \tag{24}$$

The weight functions are hence bounded by the circular arcs with $v_\perp > 0$. The center and the radius r_v are given by

$$v_{\parallel,0} = -\frac{\cos\phi E_\gamma}{(m_{pr} - m_f)c}, \tag{25}$$

$$v_{\perp,0} = \pm\frac{\sin\phi E_\gamma}{(m_{pr} - m_f)c}, \tag{26}$$

$$r_v = \sqrt{\frac{m_{pr}}{m_f}\left(\frac{E_\gamma^2}{(m_{pr} - m_f)^2c^2} + \frac{2(E_\gamma - Q)}{m_{pr} - m_f}\right)}. \tag{27}$$

The distance of the center of the circular arcs to the origin is

$$v_0 = \frac{E_\gamma}{(m_{pr} - m_f)c}. \tag{28}$$

The radicand in equation 27 must be positive which implies a minimum energy of the observable γ-rays:

$$E_\gamma \geq E_{\gamma,min} = \sqrt{2(m_{pr} - m_f)c^2Q + (m_{pr} - m_f)^2c^4} - (m_{pr} - m_f)c^2. \tag{29}$$

For example, for the D(p,γ)^{3}He reaction with fast protons and thermal deuterium $E_{\gamma,min} = 5.480$ MeV (for $Q = 5.488$ MeV). This minimum energy is only a few keV below the released energy Q whereas there are no maximum energies. The peak is strongly asymmetric with a much larger high-energy tail than low-energy tail as has been observed previously [67]. As the low-energy tail is close to the spectral resolution, we consider the nominal peak energy and the high-energy tail in the following. For NES an analogous minimum energy of observable neutrons was found to be $E_n > Q/2$ [7]

which implies a considerably more prominent low-energy tail in neutron emission energy spectra.

As observed in figure 3 and in equations 25 – 28, the radius and the distance of the center to the origin do not depend on the observation angle ϕ, but the pitch coordinate $v_\parallel/v$ of the center does. For a given energy E_γ we can now give upper and lower energy limits on the fast proton leading to the γ-ray emission. The center of the upper circular boundary has $v_{\perp,0} > 0$, whereas the center of the lower circular boundary $v_{\perp,0} < 0$ (see equation 26). Hence the largest and smallest possible proton energies E_{max} and E_{min} for a given γ-ray energy E_γ are

$$E_{min} = \frac{1}{2} m_f (r_v - v_0)^2, \tag{30}$$

$$E_{max} = \frac{1}{2} m_f (r_v + v_0)^2 \tag{31}$$

where r_v and v_0 are given by equations 27 and 28, respectively. The fast-ion energy limits for a given γ-ray energy range are found at the extremal values of the considered γ-ray energies. In figure 4 we plot an example of a probability function together with its boundaries as calculated in equations 25 – 27 as well as the upper and lower limits on the proton energies according to equations 30 and 31. In $(v_\parallel, v_\perp)$-coordinates the upper and lower energy limits show as the two circles about the origin that each touch the probability function. These upper and lower proton energy limits are plotted as a function of the measured γ-ray energy E_γ for the D(p,γ)^{3}He reaction in figure 5, illustrating the fast-ion energy resolution of the measurement for each γ-ray energy. This reaction is useful for tail temperatures $T_\perp < 400$ keV. At higher tail temperatures the peak tends to become difficult to separate from the background [18]. The energy limits are valid for zero temperature of the deuterium. We note that in JET there are often also fast deuterium ions in the plasma. Fast hydrogen is generated by first harmonic ICRH. If fast deuterium ions due to NBI are in the plasma, they will also be accelerated to high energies by second harmonic ICRH. Under some conditions fast deuterium can even be generated without NBI [18].

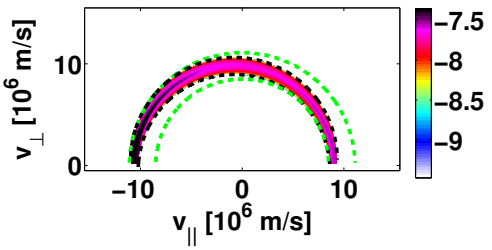

Figure 4. Probability function of D(p,γ)^{3}He with $v_p \gg v_D$ for $\phi = 30°$ and $E_{\gamma,1} - Q = 300$ keV in units [γ-photons / (ion $\times$ s)] in base ten logarithm. We set $E_{\gamma,2} - E_{\gamma,1} = 50$ keV, so that the low-energy and high-energy boundaries are more easily distinguishable. Black dashed lines: boundaries. Green dashed lines: Upper and lower energy limits.

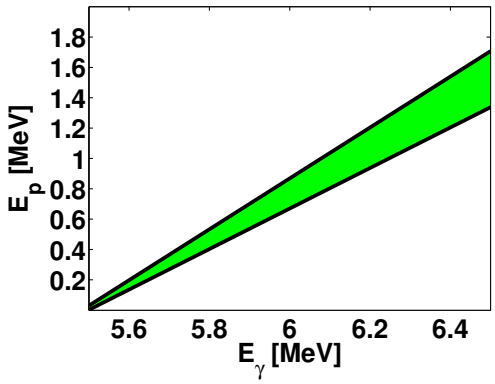

Figure 5. Proton energy resolution of the GRS measurement. The green region shows possible proton energies E_p for a given measured γ-ray energy E_γ. This neglects the energy of the thermal species. Here we set $E_{\gamma,2} - E_{\gamma,1} = 1$ keV.

The fast-ion energy resolution of the measurement is good if $r_v \gg v_0$. This is indeed the case for large or even moderate energy shifts. The ratio r_v/v_0 is

$$\frac{r_v}{v_0} = \sqrt{\frac{m_{pr}}{m_f}\left(1 + \frac{E_\gamma - Q}{E_\gamma} \times \frac{2(m_{pr} - m_f)c^2}{E_\gamma}\right)}. \tag{32}$$

At the nominal peak energy $E_\gamma = Q$, the radius becomes $r_v = \sqrt{\frac{m_{pr}}{m_f}} v_0$. This will also hold approximately when the energy shift $E_\gamma - Q$ is so small that the first term in equation 27 dominates. The second term dominates at large energy shifts, i.e. if

$$\frac{E_\gamma - Q}{E_\gamma} \gg \frac{E_\gamma}{2(m_{pr} - m_f)c^2}. \tag{33}$$

For example for fast protons in D(p,γ)^{3}He, $2(m_{pr} - m_f)c^2 \sim 4$ GeV and $E_\gamma \sim 5.5$ MeV, and hence the fraction $E_\gamma/(2(m_{pr} - m_f)c^2)$ is of order 10^{-3}. The radius is larger than the distance of the circular arc to the origin, unless the E_γ is very close to the minimum energy $E_{\gamma,min}$. For large energy shifts according to equation 33, we find $r_v \gg v_0$, i.e. the centers of the circular arcs are close to the origin compared with the radius. Equation 32 suggests that low Q-values (and hence typical $E_\gamma \sim Q$), large m_{pr}/m_f and large $m_{pr} - m_f$ are beneficial for the energy resolution. NES weight functions are analogously bounded by circular arcs. But for the GRS weight function of the D(p,γ)^{3}He reaction, the center of the circle lies very close to the origin compared with the radius. Hence for this and other selected one-step reaction GRS, the measured γ-energies can be related to particular fast-ion energies in rather narrow bands. The reaction kinematics of NES and one-step reaction GRS are very similar. The significant differences originate from the ratios between energies and momenta for neutron and γ-ray fusion products:

$$E_n = p_n \frac{v_n}{2}, \tag{34}$$

$$E_\gamma = p_\gamma c \tag{35}$$

For example, for the 2.45 MeV neutrons from D(D,n)^{3}He, $E_n/p_n \lesssim c/20$. For one-step reactions releasing γ-rays, $E_\gamma/p_\gamma = c$ as always. One may estimate how much of the

initial fast-ion momentum a released γ-ray or neutron can carry:

$$\frac{p_\gamma}{p_f} = \frac{E_\gamma}{E_f}\frac{v_f}{2c}, \tag{36}$$

$$\frac{p_n}{p_f} = \frac{E_n}{E_f}\frac{v_f}{v_n}. \tag{37}$$

As $v_n/2c \ll 1$ and if $E_n \sim E_\gamma$, the γ-rays carry a much smaller fraction of the total momentum after the reaction compared with a neutron in a similar reaction. The γ-ray therefore tends to carry a significant fraction of the energy, but a small fraction of the momentum compared with neutrons. For the D(p,γ)^{3}He reaction with $E_p \sim 1$ MeV and $E_\gamma \sim Q \sim 5.5$ MeV, we get $p_\gamma/p_p \sim 0.13$. For the D(D,γ)^{4}He reaction with $E_D \sim 1$ MeV and $E_\gamma \sim Q \sim 23.8$ MeV, we get $p_\gamma/p_D \sim 0.39$. As comparison, for the D(D,n)^{3}He reaction releasing 2.45 MeV neutrons and $E_D \sim 1$ MeV, we get $p_n/p_D \sim 1.1$. Hence the observation regions become strongly selective in energy and only weakly selective in pitch, as reflected by the circular shapes centered close to the origin, for one-step reactions releasing γ-rays with low Q-value when the momentum carried by the γ-ray is comparatively low. Examples of probability functions for various reactions illustrating their energy resolution will be shown in section 7.

6. Numerically calculated weight functions with anisotropic cross sections

Weight functions can also be calculated numerically using the GENESIS code that predicts a GRS measurement for an arbitrary fast-ion distribution function [29, 68]. In this numerical approach, we calculate a γ-ray spectrum for a collection of N_f fast ions located at a single point in velocity space and then scan the location of this point through velocity space. This formalism has been presented for two-step reaction GRS measurements [8] and is analogous to numeric computation of weight functions for FIDA [3, 11], CTS [5] and NES [6, 7]. The amplitude of the weight function at phase-space position $(\mathbf{x}_p, v_{\parallel p}, v_{\perp p})$ is [7]

$$w(E_{\gamma,1}, E_{\gamma,2}, \phi, v_{\parallel p}, v_{\perp p}, \mathbf{x}_p) = \frac{s(E_{\gamma,1}, E_{\gamma,2}, \phi)}{N_f}. \tag{38}$$

GRS weight functions show the incident rate s of γ-photons between two γ-ray energies viewed at angle ϕ per alpha particle at phase-space position $(\mathbf{x}_p, v_{\parallel p}, v_{\perp p})$. In the numerical approach we take anisotropy of the cross sections into account [71]. Figure 6 shows the rate function R for the two observation angles $\phi = 90°$ and $\phi = 30°$ illustrating the strong anisotropy of the cross sections. For isotropic cross sections the isolevels are concentric circles (see figure 1). Figure 7 shows numerically calculated weight functions at these angles. While the shapes of the numerically calculated weight functions agree with the analytic model at the same angles (see figure 3), the amplitudes are different due to the anisotropic cross sections.

Fast-ion distribution functions typical for ICRH are often characterized by a so-called tail temperature. We model the tail of such a distribution function as strongly biased bi-Maxwellian with a tail temperature $T_\perp = 150$ keV and $T_\parallel = 15$ keV as

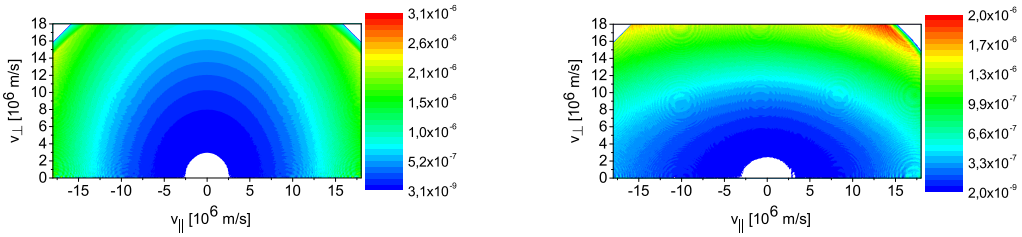

(a) $\phi = 90°$ (b) $\phi = 30°$

Figure 6. Rate function R in units [γ-photons / (ion $\times$ s)] for two observation angles. Anisotropic cross sections are accounted for.

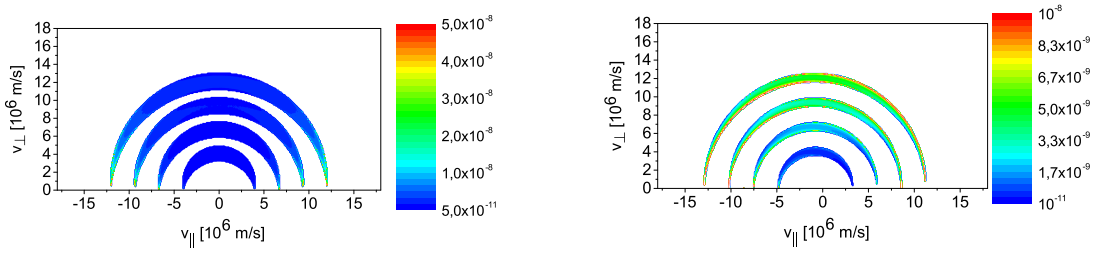

(a) $\phi = 90°$ (b) $\phi = 30°$

Figure 7. Numerically calculated weight function in units [γ-photons / (ion $\times$ s)] for two observation angles covering various energy ranges of fixed width $E_{\gamma,2} - E_{\gamma,1} = 1$ keV. From inside to outside: $E_{\gamma,1} - Q = 50$ keV, 150 keV, 300 keV, 500 keV. Anisotropic cross sections are accounted for.

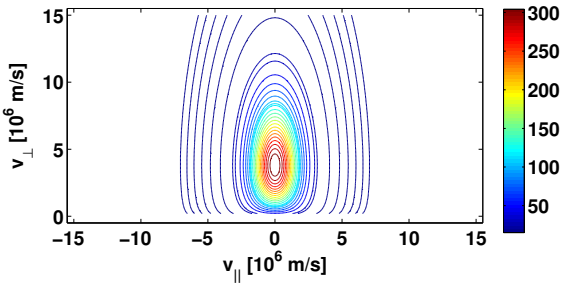

Figure 8. 2D bi-Maxwellian in units [fast ions $\times$ s^2/m^5]. The 2D bi-Maxwellian f^{2D} is related to the corresponding 3D bi-Maxwellian f^{3D} by $f^{2D} = 2\pi v_\perp f^{3D}$ assuming rotational symmetry about the magnetic field vector.

illustrated in figure 8. The product of weight functions and a given fast-ion velocity distribution functions $w \times f$ resolves the origin of the γ-rays in 2D velocity space of the fast ions for this given f as illustrated in figure 9. The narrow probability functions at $\phi = 30°$ provide a better energy resolution for narrow velocity distribution functions with $v_\parallel \ll v_\perp$, such as the bi-Maxwellian from figure 8.

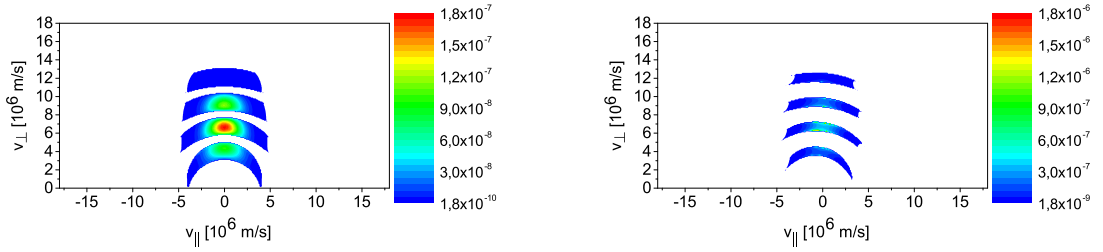

(a) $\phi = 90°$ (b) $\phi = 30°$

Figure 9. Products $w \times f$ of the weight functions illustrated in figure 7 and the bi-Maxwellian illustrated in figure 8. The observation angles are (a) $\phi = 90°$ and (b) $\phi = 30°$. The γ-rays observed in each narrow energy range originate from small regions in velocity space.

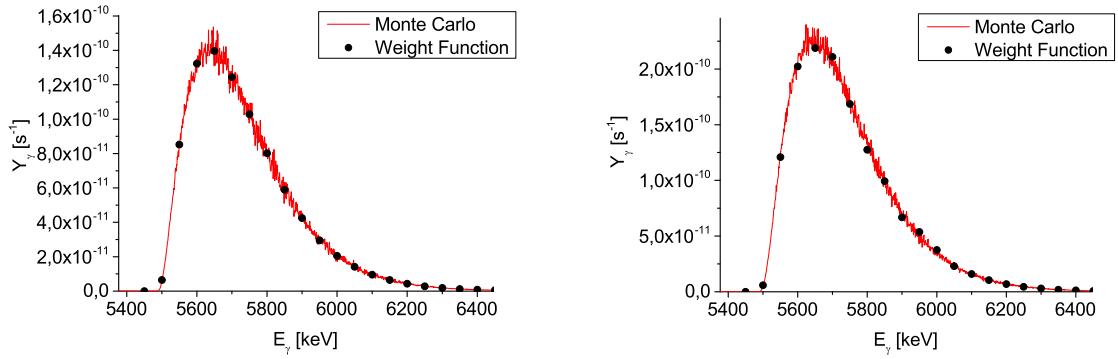

(a) $\phi = 90°$ (b) $\phi = 30°$

Figure 10. Energy spectra for the bi-Maxwellian distribution from figure 8 as calculated using Monte Carlo simulations and by weight functions for (a) $\phi = 90°$ and (b) $\phi = 30°$. The spectrum shows the number of detected γ-photons per second [photons/s] in small energy bins of widths $E_{\gamma,2} - E_{\gamma,1} = 1$ keV.

Figure 10 shows spectra as calculated by traditional Monte Carlo simulations and by weight functions. The energy and momentum of the thermal species are here neglected. As expected, the two approaches give very similar results and differ only due to Monte Carlo noise. The weight function approach has two advantages. First, the velocity-space region generating the γ-ray at each energy can be identified (see figure 9). Second, once the weight functions are calculated, the weight function approach is significantly faster

as it requires only a matrix multiplication instead of Monte Carlo simulations. Hence spectra of many fast-ion velocity distribution functions can rapidly be calculated.

7. Other reactions and excited charged reaction products

Our formalism is general and applies to any one-step reaction GRS measurement, including reactions where the charged reaction product has an intrinsic mass width. This leads to so-called intrinsic broadening of the reaction energy peak such as in D(T,γ)^{5}He. For many reactions the energy dependence of the reaction cross sections is described by only few data points. We can nevertheless draw conclusions about the velocity-space sensitivity for such one-step reactions. The cross sections enter only into the calculation of the rate function R whereas probability functions are calculated based on the conservation of energy and momentum and do not depend on the cross sections. Hence we can calculate the probability functions and the boundaries of weight functions exactly even if the cross sections are poorly known. Three examples of one-step reactions with less well established cross sections are D(D,γ)^{4}He, D(T,γ)^{5}He and T(p,γ)^{4}He. The highly energetic γ-rays from these reactions (see table 1) could be observable at ITER as deuterium and tritium are the main constituents of ITER plasmas and the continuum emission above 10 MeV in ITER is practically zero.

Some example probability functions of the D(p,γ)^{3}He, D(D,γ)^{4}He and T(p,γ)^{4}He reactions are illustrated in figure 11. The D(p,γ)^{3}He reactions with fast protons provides the narrowest weight functions suggesting direct fast-proton energy resolution. D(p,γ)^{3}He with fast deuterium and thermal protons (as might be useful in the low-activation phase of ITER with hydrogen plasmas and deuterium beam injection) and T(p,γ)^{4}He have somewhat broader weight functions tilted towards negative pitches. The D(D,γ)^{4}He reaction provides the lowest fast-ion energy resolution.

Reactions with so-called intrinsic broadening require special attention, for example the D(T,γ)^{5}He reaction. The ground state of the ^{5}He nucleus has a broad energy width due to its very short lifetime after which it decays to ^{4}He and a neutron. The energy of the ground state is then defined as Lorentzian with a width $\sigma_Q^* = 0.648$ MeV obeying the uncertainty principle. In this case DT gamma-ray energies also follow a Lorentzian distribution centered about the nominal energy $Q = 16.85$ MeV:

$$\mathrm{pdf}(Q^*) = \frac{1}{\pi}\frac{\frac{1}{2}\sigma_Q^*}{(Q-Q^*)^2 + (\frac{1}{2}\sigma_Q^*)^2}. \tag{39}$$

We account for this effect by introducing Q^* as nuisance parameter:

$$\begin{aligned} &\mathrm{prob}(E_{\gamma,1} < E_\gamma < E_{\gamma,2}|\phi, v_\parallel, v_\perp) \\ &= \int_{Q^*} \mathrm{prob}(E_{\gamma,1} < E_\gamma < E_{\gamma,2}|\phi, v_\parallel, v_\perp, Q^*) \times \mathrm{pdf}(Q^*)dQ^* \\ &= \int_{Q^*} \left|\frac{\Gamma_2(Q^*,..) - \Gamma_1(Q^*,..)}{\pi}\right| \mathrm{pdf}(Q^*)dQ^*. \end{aligned} \tag{40}$$

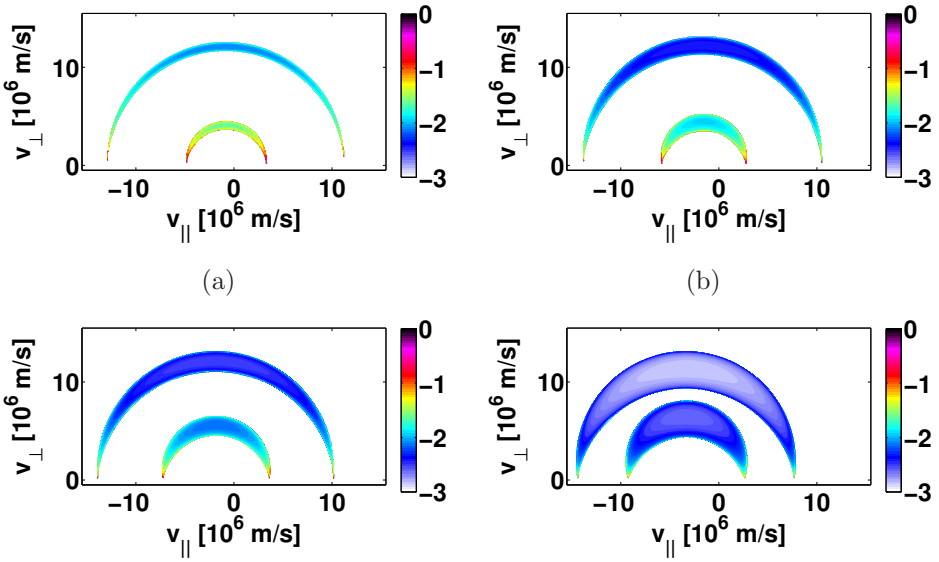

Figure 11. Probability functions prob($E_{\gamma,1} < E_\gamma < E_{\gamma,2}|\phi, v_\parallel, v_\perp$) for the various reactions: (a) D(p,γ)^{3}He with fast p; (b) D(p,γ)^{3}He with fast D; (c) T(p,γ)^{4}He with fast p; (d) D(D,γ)^{4}He. The inner probability functions is at $E_{\gamma,1} - Q = 50$ keV for each reaction, and the outer at 500 keV. The observation angle is $\phi = 30°$, and $E_{\gamma,2} - E_{\gamma,1} = 1$ keV.

An example probability function for the D(T,γ)^{5}He reaction is shown in figure 12. The intrinsic broadening of the peak broadens the observable velocity space, such that ions with any energy could result in the given γ-ray energy. Nevertheless, the measurement is significantly more sensitive in some regions compared with others.

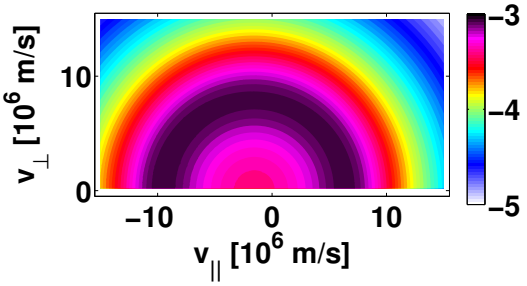

Figure 12. Probability function prob($E_{\gamma,1} < E_\gamma < E_{\gamma,2}|\phi, v_\parallel, v_\perp$) of the D(T,$\gamma$)^{5}He reaction for $\phi = 30°$, $E_{\gamma 1} - Q = 0.35$ MeV, $E_{\gamma 2} - E_{\gamma 1} = 1$ keV. The intrinsic width of the line is 648 keV.

8. Blurring due to high temperatures

In our model we assumed that the energy and momentum of the thermal species is negligible. Non-zero temperatures can be accounted for by the Monte-Carlo sampling approach as previously shown for NES [7] where it was found that non-zero temperatures

blur the weight functions. In figure 13 we illustrate the blurring effect for one-step reaction GRS weight functions for a typical JET ion temperature of 5 keV. The blurring due to thermal broadening decreases the fast-ion energy resolution, but some energy resolution can still be provided at these typical temperatures. The strength of the blurring can be assessed by comparing the momenta and energies of the fast ions to those of the thermal reaction partners. Our analytical model from section 2 neglected the energies and momenta of the thermal ions (equations 4-7). These approximations improve with the fast-ion velocity at given temperature. This suggests that at larger fast-ion energies the blurring effect is less pronounced and the fast-ion energy resolution thus less affected.

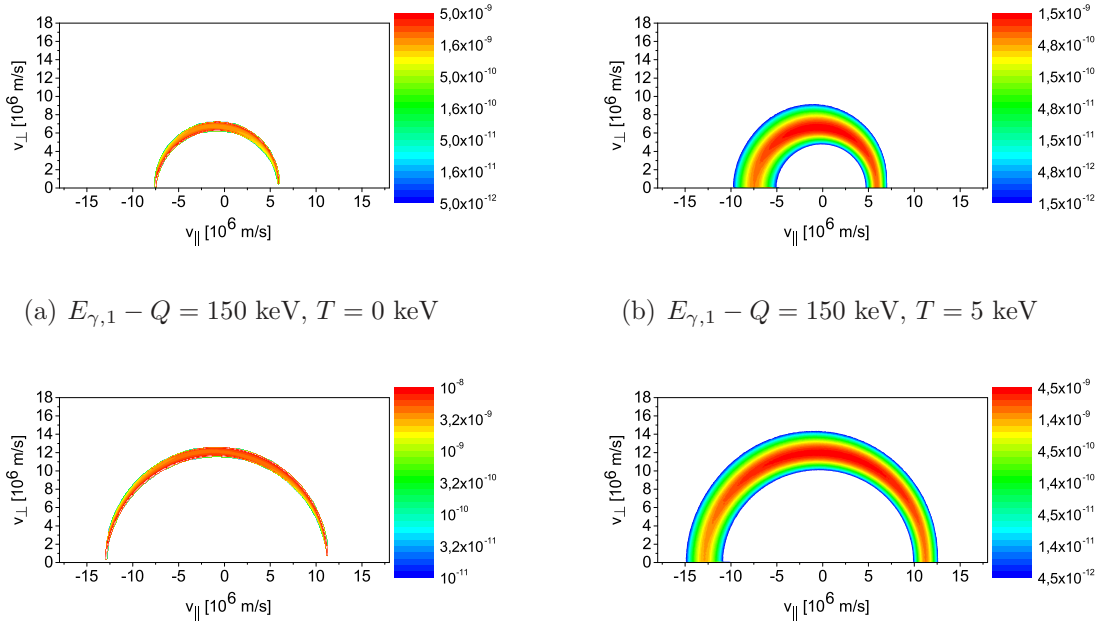

(a) $E_{\gamma,1} - Q = 150$ keV, $T = 0$ keV

(b) $E_{\gamma,1} - Q = 150$ keV, $T = 5$ keV

(c) $E_{\gamma,1} - Q = 500$ keV, $T = 0$ keV

(d) $E_{\gamma,1} - Q = 500$ keV, $T = 5$ keV

Figure 13. Comparison of numerically calculated weight functions at 0 keV and 5 keV at two γ-ray energy shifts $E_{\gamma,1} - Q$.

9. Discussion

Weight functions have previously been calculated for FIDA [3, 4], NPA [3], CTS [4, 5], FILD [43] and NES measurements [6, 7] as well as for two-step reaction GRS [8]. The substantial differences between the weight functions of each diagnostic imply that the diagnostics complement each other well. FIDA, CTS, NES and two-step reaction GRS observe large regions in velocity space which do not allow energy resolution of the measurements unless tomographic techniques in velocity space are used [9–13]. In contrast, the velocity-space positions of the narrow weight functions of selected one-step reaction GRS measurements demonstrate that GRS can provide energy resolution

of the fast-ion population, even without tomographic techniques. The fast-ion energy resolution is a strong asset of one-step reaction high resolution GRS measurements that could be highly important for further fast-ion studies at JET, ITER or other large-size tokamaks with significant γ-ray fluxes. However, the temperature should be as low as possible for good energy resolution. Figure 13 illustrates that the fast-ion energy resolution at a plasma temperature of 5 keV is degraded compared with the 0 keV case. This temperature is likely the upper limit for useful energy resolution. At the very high temperatures of burning plasmas ($T \sim 20$ keV), it is likely that tomographic inversion techniques will be required to provide useful energy resolution.

We have argued that the ITER measurement requirements on resolution of the confined α-particle energies [2] are not achievable by major core fast-ion diagnostics (FIDA [56, 65], CTS [72, 73], NES [7, 32] or two-step reaction GRS [7, 32]) without resorting to tomographic inversion in velocity space. A notable exception is NPA that can provide good energy resolution for a narrow observed pitch range if the signal-to-noise ratio is high enough. Our results would suggest that energy resolution of confined α-particles could in principle be achievable at moderate temperatures for one-step reactions involving α-particles. However, the chances to observe such peaks at ITER are bleak. The capture reactions $\alpha(\mathrm{D},\gamma)^6\mathrm{Li}$ and $\alpha(\mathrm{T},\gamma)^7\mathrm{Li}$ have much lower cross sections than $^9\mathrm{Be}(\alpha, \mathrm{n}\gamma)^{12}\mathrm{C}$ by about five to six orders of magnitude at the resonances. As deuterium and tritium will be about 100 times more abundant than beryllium in ITER and the velocity-space observation regions have comparable sizes, the emission will be about three to four orders of magnitude smaller. We can expect counting rates on the order of 1 Hz in a spectral range (1-3 MeV) where the background counting rates are on the order of 100 kHz. Hence the observation of one-step reaction peaks involving α-particles at ITER will be extremely difficult if not impossible. Hence one-step reaction GRS will likely not be able to meet the ITER measurement requirement on energy resolution of confined α-particles either. Nevertheless, other fast ions should be readily observable at ITER and DEMO. $\mathrm{T}(\mathrm{p},\gamma)^4\mathrm{He}$ has been highlighted as a very promising reaction in DT plasmas [35] as may be demonstrated using ICRH minority heating in the upcoming tritium campaign at JET. The $\mathrm{D}(\mathrm{T},\gamma)^5\mathrm{He}$ reaction should be observable, as count rates on the order of 1 kHz are expected in a high-energy spectral range (> 10 MeV) where the background is practically zero. Other ions accelerated by ion cyclotron resonance heating, e.g. ^{3}He, could also be readily observable. The $\mathrm{D}(\mathrm{D},\gamma)^4\mathrm{He}$ reaction peak could so far not be detected in JET discharges, but might appear at ITER.

Weight functions are now available for all major core fast-ion diagnostics. At ASDEX Upgrade [74], full tomographic inversion of fast-ion measurements to infer fast-ion distribution functions based on weight functions has already been demonstrated [11]. Such a full tomographic inversion is not likely to be achievable based on one-step reaction GRS measurements by themselves. However, ASDEX Upgrade has up to six FIDA views [56, 62, 65], two CTS views [55, 63, 75–78] one NES view [79, 80], one GRS view [41], one NPA [81] as well as three FILD diagnostics [82, 83]. We can in principle

combine the one-step reaction GRS with the other fast-ion measurements [10, 84]. This approach is also promising for JET which is equipped with two NES views, two GRS views as well as an NPA [31, 32]. Lastly, we will be able to show the velocity-space sensitivity of GRS measurements at ITER [34] and DEMO [35]. ITER will be equipped with GRS, NES [2] and CTS [85–87] as well as fast-ion charge-exchange recombination spectroscopy [88]. With this set of diagnostics, measurements of the 2D fast-ion velocity distribution functions on ITER, and hence energy resolution, should be in reach.

10. Conclusions

We derived analytic expressions, so-called weight functions, describing the velocity-space observation regions of one-step reaction GRS measurements. The spectral resolution of the γ-rays achievable with modern detectors allows energy resolution of the fast ion distribution for all pitches for selected one-step reactions at moderate plasma temperatures. One-step reaction GRS is the only major core fast-ion diagnostic that can provide energy resolution directly without tomographic inversion in velocity space which is a strong asset of this diagnostic. The D(p,γ)^{3}He reaction with fast protons has the best direct energy resolution. The D(D,γ)^{4}He allows somewhat coarser energy resolution. The direct energy resolution is worst for reactions with intrinsic broadening. High plasma temperatures as expected in ITER also strongly degrade the direct energy resolution. Nevertheless, one-step reaction GRS weight functions provide additional information on fast-ion velocity space for any machine with substantial γ-ray fluxes, such as JET, ITER and DEMO. Weight functions are now available for the major fast-ion diagnostics: FIDA, NPA, CTS, NES, and one- and two-step reaction GRS. Hence all major fast-ion diagnostics can now in principle be combined to determine fast-ion velocity distribution functions experimentally.

Acknowledgments

This work has been carried out within the framework of the EUROfusion Consortium and has received funding from the Euratom research and training programme 2014-2018 under grant agreement No 633053. The views and opinions expressed herein do not necessarily reflect those of the European Commission.

References

[1] Romanelli F 2015 *Nucl. Fusion* **55** 104001
[2] Donné A J H *et al* Progress in the ITER Physics Basis Chapter 7: Diagnostics 2007 *Nucl. Fusion* **47** S337–S384
[3] Heidbrink W W *et al* 2007 *Plasma Phys. Control. Fusion* **49** 1457–1475
[4] Salewski M *et al* 2014 *Plasma Phys. Control. Fusion* **56** 105005
[5] Salewski M *et al* 2011 *Nucl. Fusion* **51** 083014
[6] Jacobsen A S *et al* 2014 *Rev. Sci. Instrum.* **85** 11E103
[7] Jacobsen A S *et al* 2015 *Nucl. Fusion* **55** 053013

[8] Salewski M *et al* 2015 *Nucl. Fusion* **55** 093029
[9] Salewski M *et al* 2012 *Nucl. Fusion* **52** 103008
[10] Salewski M *et al* 2013 *Nucl. Fusion* **53** 063019
[11] Salewski M *et al* 2014 *Nucl. Fusion* **54** 023005
[12] Salewski M *et al* 2015 *Plasma Phys. Control. Fusion* **57** 014021
[13] Jacobsen A S *et al* 2016 *Plasma Phys. Control. Fusion* at press
[14] Kiptily V G *et al* 2006 *Plasma Phys. Control. Fusion* **48** R59–R82
[15] Tardocchi M *et al* 2013 *Plasma Phys. Control. Fusion* **55** 074014
[16] Boyd D A *et al* 1989 *Nucl. Fusion* **29** 593–604
[17] Jarvis O N *et al* 1996 *Nucl. Fusion* **36** 1513–1530
[18] Kiptily V G *et al* 2002 *Nucl. Fusion* **42** 999–1007
[19] Kiptily V G *et al* 2003 *Rev. Sci. Instrum.* **74** 1753
[20] Kiptily V G *et al* 2004 *Phys. Rev. Lett.* **93** 115001
[21] Kiptily V G *et al* 2005 *Nucl. Fusion* **45** L21–L25
[22] Kiptily V G *et al* 2009 *Nucl. Fusion* **49** 065030
[23] Kiptily V G *et al* 2012 *Plasma Phys. Control. Fusion* **54** 074010
[24] Kiptily V G *et al* 2013 *Plasma Fus. Res.* **8** 2502071
[25] Kiptily V G *et al* 2010 *Nucl. Fusion* **50** 084001
[26] Murari A *et al* 2010 *Rev. Sci. Instrum.* **81** 10E136
[27] Nocente M *et al* 2010 *Rev. Sci. Instrum.* **81** 10D321
[28] Nocente M *et al* 2012 *Nucl. Fusion* **52** 063009
[29] Tardocchi M *et al* 2011 *Phys. Rev. Lett.* **107** 205002
[30] Shevelev A E *et al* 2013 *Nucl. Fusion* **53** 123004
[31] Eriksson J *et al* 2015 *Nucl. Fusion* **55** 123026
[32] Schneider M *et al* 2016 *submitted* Modelling third harmonic Ion Cyclotron acceleration of deuterium beams for JET Fusion Product Studies Experiments
[33] Romanelli F 2013 *Nucl. Fusion* **53** 104002
[34] Chugunov I N *et al* 2011 *Nucl. Fusion* **51** 083010
[35] Kiptily V 2015 *Nucl. Fusion* **55** 023008
[36] Newman D E and Cecil F 1984 *Nucl. Instrum. Meth. Phys. Res. A* **227** 339–341
[37] Cecil F E and Medley S S 1988 *Nucl. Instrum. Meth. Phys. Res. A* **271** 628–635
[38] Kondoh T *et al* 1997 *J. Nucl. Mat.* **241-243** 564–568
[39] Nishitani T *et al* 2001 *Rev. Sci. Instrum.* **72** 877
[40] Nocente M *et al* 2013 *IEEE Trans. Nucl. Sci.* **60** 1408–1415
[41] Nocente M *et al* 2012 *Nucl. Fusion* **52** 094021
[42] Kiptilyj V G 1990 *Fusion Sci. Tech.* **18** 583–590
[43] Pace D C *et al* 2012 *Rev. Sci. Instrum.* **83** 073501
[44] Heidbrink W W 2010 *Rev. Sci. Instrum.* **81** 10D727
[45] Geiger B *et al* 2014 *Nucl. Fusion* **54** 022005
[46] Heidbrink W W *et al* 2006 *Rev. Sci. Instrum.* **77** 10F120
[47] Luo Y *et al* 2007 *Rev. Sci. Instrum.* **78** 033505
[48] Podestà M *et al* 2008 *Rev. Sci. Instrum.* **79** 10E521
[49] Van Zeeland M A *et al* 2009 *Plasma Phys. Control. Fusion* **51** 055001
[50] Van Zeeland M A *et al* 2010 *Nucl. Fusion* **50** 084002
[51] Bortolon A *et al* 2010 *Rev. Sci. Instrum.* **81** 10D728
[52] Heidbrink W W *et al* 2011 *Plasma Phys. Control. Fusion* **53** 085007
[53] Michael C A *et al* 2013 *Plasma Phys. Control. Fusion* **55** 095007
[54] Heidbrink W W *et al* 2014 *Plasma Phys. Control. Fusion* **56** 095030
[55] Nielsen S K *et al* 2015 *Plasma Phys. Control. Fusion* **57** 035009
[56] Geiger B *et al* 2015 *Plasma Phys. Control. Fusion* **57** 014018
[57] Heidbrink W W *et al* 2008 *Rev. Sci. Instrum.* **79** 10E520

[58] Podesta M *et al* 2009 *Physics of Plasmas* **16** 056104
[59] Garcia-Munoz M *et al* 2011 *Nucl. Fusion* **51** 103013
[60] Geiger B *et al* 2011 *Plasma Phys. Control. Fusion* **53** 065010
[61] Muscatello C M *et al* 2012 *Plasma Phys. Control. Fusion* **54** 025006
[62] Geiger B *et al* 2013 *Rev. Sci. Instrum.* **84** 113502
[63] Rasmussen J *et al* 2015 *Plasma Phys. Control. Fusion* **57** 075014
[64] Pace D C *et al* 2013 *Physics of Plasmas* **20** 056108
[65] Geiger B *et al* 2015 *Nucl. Fusion* **55** 083001
[66] Weiland M *et al* 2016 *Plasma Phys. Control. Fusion* **58** 025012
[67] Nocente M *et al* 2015 *Nucl. Fusion* **55** 123009
[68] Nocente M 2012 *Neutron and gamma-ray emission spectroscopy as fast ion diagnostics in fusion plasmas* Ph.D. thesis URL `https://boa.unimib.it/handle/10281/28397`
[69] Burbidge E M *et al* 1957 *Rev. Mod. Phys.* **29** 547–650
[70] Bosch H S and Hale G 1992 *Nucl. Fusion* **32** 611–631
[71] Proverbio I *et al* 2010 *Rev. Sci. Instrum.* **81** 10D320
[72] Moseev D *et al* 2011 *Plasma Phys. Control. Fusion* **53** 105004
[73] Nishiura M *et al* 2014 *Nucl. Fusion* **54** 023006
[74] Stroth U *et al* 2013 *Nucl. Fusion* **53** 104003
[75] Meo F *et al* 2008 *Rev. Sci. Instrum.* **79** 10E501
[76] Meo F *et al* 2010 *J. Phys.: Conf. Ser.* **227** 012010
[77] Salewski M *et al* 2010 *Nucl. Fusion* **50** 035012
[78] Furtula V *et al* 2012 *Rev. Sci. Instrum.* **83** 013507
[79] Tardini G *et al* 2012 *J. Instrum.* **7** C03004–C03004
[80] Tardini G *et al* 2013 *Nucl. Fusion* **53** 063027
[81] Schneider P A *et al* 2015 *Rev. Sci. Instrum.* **86** 073508
[82] Garcia-Munoz M *et al* 2013 *Nucl. Fusion* **53** 123008
[83] Garcia-Munoz M *et al* 2013 *Plasma Phys. Control. Fusion* **55** 124014
[84] Jacobsen A S *et al* 2016 *Plasma Phys. Control. Fusion* at press
[85] Salewski M *et al* 2008 *Rev. Sci. Instrum.* **79** 10E729
[86] Salewski M *et al* 2009 *Plasma Phys. Control. Fusion* **51** 035006
[87] Salewski M *et al* 2009 *Nucl. Fusion* **49** 025006
[88] Kappatou A *et al* 2012 *Nucl. Fusion* **52** 043007